Influence of Mesoscale Topography on Tropical Cyclone Tracks: Further Examination of the Channeling Effect

CHUN-CHIEH WU, TSUNG-HAN LI, AND YI-HSUAN HUANG

Department of Atmospheric Science, National Taiwan University, Taipei, Taiwan

(Manuscript received 9 June 2014, in final form 9 April 2015)

ABSTRACT

Observations have documented typhoons experiencing pronounced track deflection before making landfall in Taiwan. In this study, idealized full-physics model experiments are conducted to assess the orographic influence on tropical cyclone (TC) track. An intense and westward-moving TC is simulated to approach the bell-shaped terrain imitating the Taiwan topography. Sensitivity numerical experiments are carried out to evaluate the topographic effect under different flow regimes and parameters, such as TC intensity, terrain height, and incident angle of the TC movement toward the topography. All the presented simulated storms experience southward track deflection prior to landfall. Different from the mechanism related to the channeling-effect-induced low-level northerly jet as suggested in previous studies, this study indicates the leading role of the northerly asymmetric flow in the midtroposphere in causing the southward deflection of the simulated TC tracks. The midtropospheric northerly asymmetric flow forms as a result of the wind speeds restrained east of the storm center and winds enhanced/maintained west of the storm center. In all, this study highlights a new mechanism that contributes to the terrain-induced southward track deflection in addition to the traditional channeling effect.

1. Introduction

The landfall of tropical cyclones (TCs) is often accompanied by heavy rain, strong winds, and destructive floods, which makes accurate prediction of TC intensity, structure, and track an urgent and important issue. Taiwan, under frequent TC threat, is a mountainous island where the summit of the Central Mountain Range (CMR) exceeds 3000 m and complicated topography covers a horizontal scale of 150 km in width and 400 km in length. The highly complicated orographic influence on typhoon tracks, circulation, and the precipitating systems in Taiwan has always been an active research topic (Wu and Kuo 1999; Wu 2013).

Both observational and numerical studies have shown that a TC would occasionally experience significant track deflection when passing over a mesoscale mountain range. Observational studies (Brand and Blelloch 1974; Wang 1980; Yeh and Elsberry 1993; Hsu et al. 2013) have assessed the statistical behavior of TC movement near Taiwan and the concurrent changes in the TC intensity and structure. For instance, Yeh and Elsberry (1993), examining 103 westward-moving typhoons near Taiwan between 1947 and 1990, found that weaker and slower TCs tend to experience greater track deflection probably as a result of larger influence and longer impact time. However, analyses in the observational studies were less informative regarding the relative importance of synoptic-scale systems and the terrain in the identified TC track deflection.

Numerical simulation studies on the terrain-induced TC track deflection, a useful approach if with proper design, can be classified into studies of real cases (e.g., Wu 2001; Jian and Wu 2008; Huang et al. 2011) and idealized experiments (Chang 1982; Bender et al. 1987; Yeh and Elsberry 1993; Lin et al. 1999; Wu and Kuo 1999; Kuo et al. 2001; Lin et al. 2005; Lin and Savage 2011; Huang et al. 2011; Hsu et al. 2013; Tang and Chan 2013). Numerical simulations with idealized settings, used in many previous studies, have provided insights into the terrain-induced changes in TC movement under

Corresponding author address: Chun-Chieh Wu, Department of Atmospheric Science, National Taiwan University, No. 1, Sec. 4, Roosevelt Rd., Taipei 106, Taiwan.
E-mail: cwu@typhoon.as.ntu.edu.tw

DOI: 10.1175/JAS-D-14-0168.1

TABLE 1. A summary of the conducted MM5 idealized experiments.

Experiment	Terrain	Tropical cyclone	Sensitivity to
CTL	Idealized bell shape, 3000 m in height	Idealized TC	Presence of topography
OC-CTL	Ocean, no terrain	As in CTL	
H10	As in CTL, but for a height of 1000 m	As in CTL	Topography height
H50	As in CTL, but for a height of 5000 m	As in CTL	
A75	As in CTL, but for a 50% width	As in CTL	Topography width [a in Eq. (3)]
A300	As in CTL, but for a doubled width	As in CTL	
B200	As in CTL, but for a 50% length	As in CTL	Topography length [b in Eq. (3)]
B600	As in CTL, but for a 150% length	As in CTL	
$I + 15$	As in CTL, but rotated 15° counterclockwise	As in CTL	Incident angle at which the vortex approaches topography
$I - 15$	As in CTL, but rotated 345° counterclockwise	As in CTL	
H2N	As in CTL, but 1° latitude to the south	As in CTL	Initial latitudinal position of the vortex center
H2S	As in CTL, but 1° latitude to the north	As in CTL	
T27	As in CTL	Weaker TC	TC intensity (still an intense TC)
T27-OC	As in OC-CTL	Weaker TC	
SML	As in CTL	Smaller-RMW TC	Radius of maximum wind
SML-OC	As in OC-CTL	Smaller-RMW TC	
LGE	As in CTL	Larger-RMW TC	
LGE-OC	As in OC-CTL	Larger-RMW TC	
SLW	As in CTL	Slow-moving TC	Vortex translation speed
SLW-OC	As in OC-CTL	Slow-moving TC	
MED	As in CTL	Medium-moving TC	
MED-OC	As in OC-CTL	Medium-moving TC	
FST	As in CTL	Fast-moving TC	
FST-OC	As in OC-CTL	Fast-moving TC	

different flow and parameter regimes. An idealized numerical simulation with 60-km horizontal resolution and seven vertical layers was carried out to understand the terrain-induced track deflection of a westward-moving TC in Chang (1982). It was suggested that a TC would make a northward turn in its path following the additional cyclonic circulation, which is induced by the cumulus heating near the terrain. With a model resolution of 45 km, Yeh and Elsberry (1993) also conducted idealized simulations to examine the effects of topography on TCs with different initial positions, background flow speed, and storm intensity. The numerical results were consistent with their observational analysis.

A dry and frictionless model and a family of nondimensional parameters were utilized to identify the flow regimes under which the terrain-induced

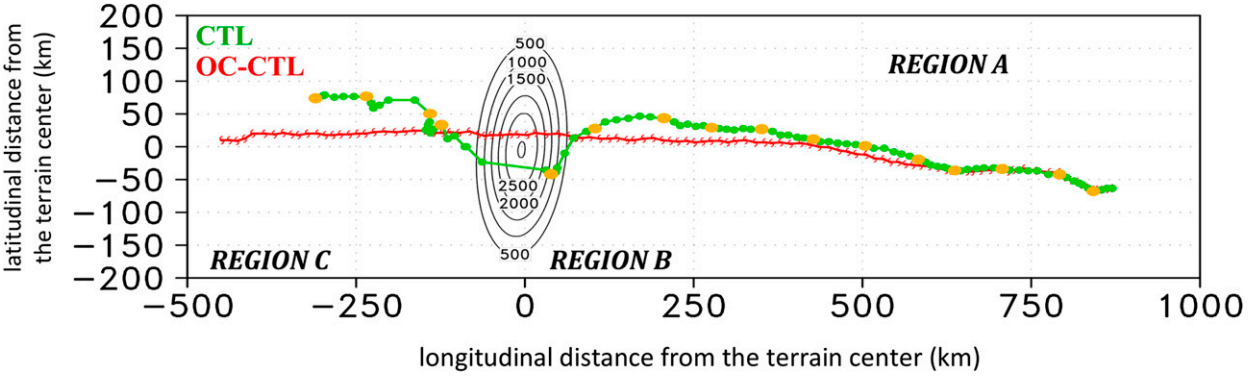

FIG. 1. Simulated TC tracks (green for CTL and red for OC-CTL) are overlaid on the terrain height contours (black; interval of 500 m) employed in CTL. The TC center position is marked every hour and highlighted by a larger solid circle every 6 h. The ordinate and abscissa show the latitudinal and longitudinal distance (km) from the terrain's geographical center, respectively. Regions A, B, and C are referred to as the regions where the storm in CTL is deflected toward the north upstream of the topography, toward the south prior to and after the landfall, and toward the north again after leaving the topography, respectively.

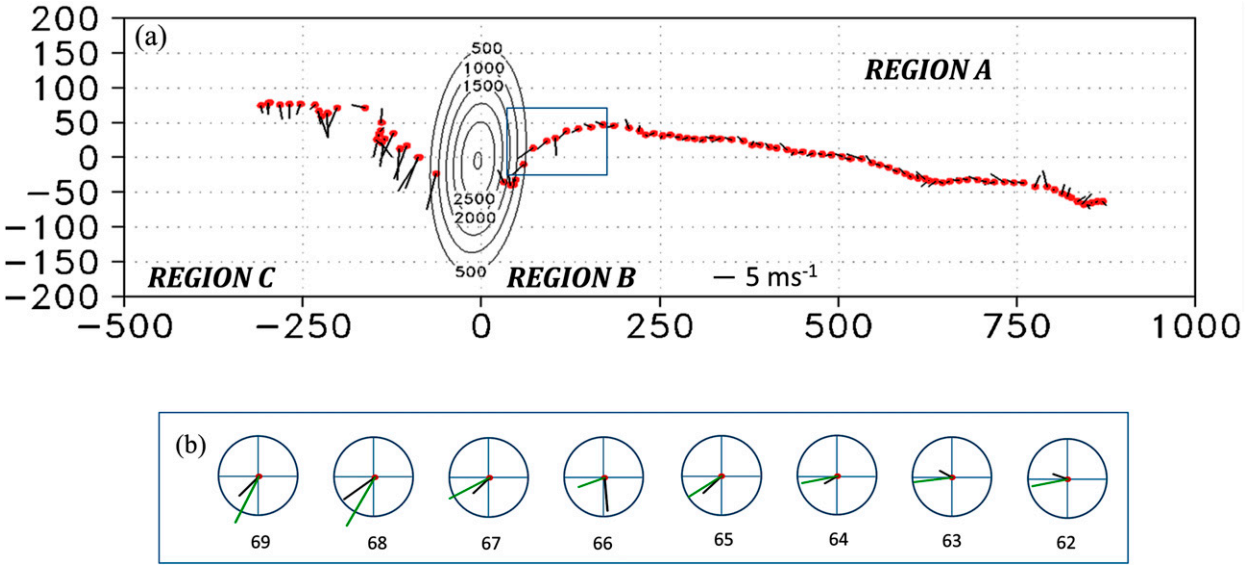

FIG. 2. (a) The red solid circles are the hourly positions of the TC center in CTL, superposed with the deep-layer ($\sigma = 0.825$–0.325) areal-mean asymmetric flow (black lines) that is calculated within 100-km radius around the storm center. (b) The black lines are as in (a), additionally overlaid with the TC motion vectors (green lines). It focuses on the time period when the storm makes a southward turn [indicated by the box in (a) as well]. The blue circles in (b) indicate the magnitude of 3 m s^{-1}.

discontinuity or deflection of TC tracks occurs (Lin et al. 2005). It was found that TC tracks tend to be discontinuous and more deflected with small values of Froude numbers (Fr = U/Nh for basic flow; Fr = V_{max}/Nh for the vortex), Rossby number (Ro = U/fL_x for basic flow; Ro = V_{max}/fR for the vortex) and the ratio of the vortex scale to the mountain range in a direction perpendicular to basic flow (R/L_y), and/or a large value of steepness of the prescribed mountain (h/L_x).[1] This parameter regime was suggested as being useful in measuring orographic blocking, which was presented as a major explanation for track deflection in Lin et al. (2005, their Fig. 12) and Lin (2007, their Fig. 5.36). The southward track deflection occurs when aforementioned parameters correspond to conditions in which a vortex experiences topographic influence and when R/L_y is particularly small. Such southward track deflection was explained by a pronounced orographic blocking effect on basic flow, a stretching (shrinking) air column in the windward (leeward) side of the terrain [Fig. 5.36a of Lin (2007)], and vorticity advection due to the channeling effect in Lin et al. (1999).

Using a sophisticated full-physics model, Jian and Wu (2008) investigated the looping motion of Super Typhoon Haitang (2005) prior to its landfall in Taiwan. It was demonstrated that Haitang's southward deflection could be attributed to the channeling effect, which is characterized by low-level wind acceleration over the confined region between the storm center and the terrain where air parcels of the swirling wind are forced to converge. These accelerated low-level winds between the storm center and the terrain thus contribute to the formation of the northerly steering flow near the inner core of the TC and push the TC southward. The investigation on the southward track deflection of Typhoon Krosa (2007) in Huang et al. (2011) showed results generally consistent with findings of Jian and Wu (2008). Huang et al. (2011) further conducted a series of idealized simulations with sophisticated physical processes at 3-km horizontal resolution to identify the key mechanisms leading to the terrain-induced track deflection for vortices approaching different locations of the topography. Results demonstrated the important role of the channeling effect in advecting an intense typhoon to the south, generally in good agreement with findings of Jian and Wu (2008).

The southward track deflection that some intense typhoons experienced when getting close to the Taiwan topography has been noted and investigated in a number of recent studies (e.g., Jian and Wu 2008; Huang et al. 2011; Hsu et al. 2013). It has been shown that although a

[1] U is the basic flow speed, N is the Brunt–Väisälä frequency, h is the mountain height, f is the Coriolis parameter, L_x is for the topography width, V_{max} is the maximum tangential wind, R is the radius of the maximum wind, and L_y is the topography length.

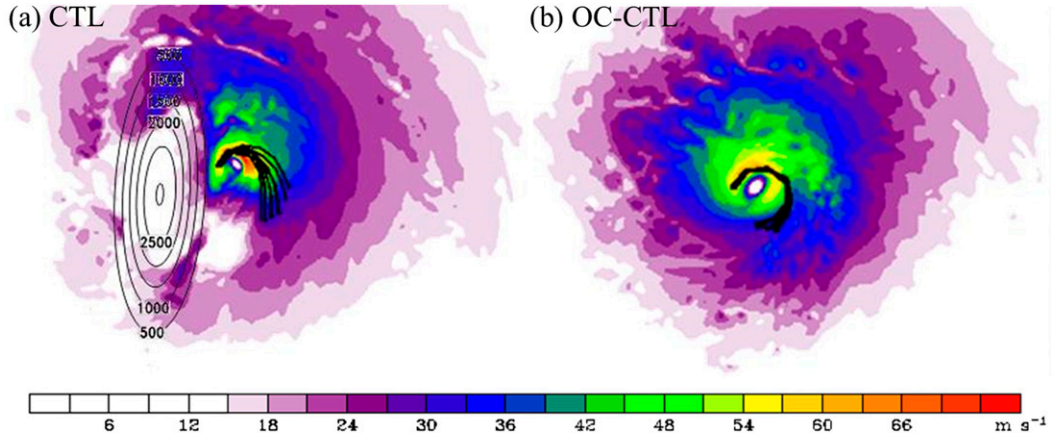

FIG. 3. Backward trajectories retrieved by the RIP4 are overlaid on the simulated 850-hPa wind speed (shaded) for (a) CTL and (b) OC-CTL. Air parcels are released between the TC center and terrain at 800 hPa at 66 h, when the storm is in region B, and calculated backward for 1 h.

TC would deflect to the north under the influence of topography during the earlier period, it would start to deflect to the south just before landfall. It is noteworthy that the southward TC track deflection documented in observations or captured in the numerical simulations is mostly for more intense TCs, suggesting that tracks of intense TCs could also be profoundly affected by the presence of mesoscale topography, such as the terrain of Taiwan.

As a follow-up study of Huang et al. (2011), this work attempts to further assess the orographic influence on TC track deflection, in particular to re-examine robustness of the channeling effect. A full-physics model with fine grid spacing is utilized to understand the role of topography in TC track deflection. While Huang et al. (2011) only examined the sensitivity to the initial latitudinal position of the vortex, this study investigates sensitivities to more parameters and flow regimes, such as the terrain height, incident angle of TC movement toward the terrain, TC intensity, and translation speed. A series of idealized simulations are conducted to investigate how the terrain impacts TC motion under different configurations of mountain range, height and shape, vortex intensity and structure, the incident angle of a moving vortex toward the mountain, initial latitudinal position of the vortex center, and storm translation speed. Model description and experiment design are described in section 2. In sections 3 and 4, the result of the control experiment and sensitivity experiments are presented respectively. The impact of the channeling effect is discussed and a new mechanism responsible for the terrain-induced southward track deflection is presented. The role of the channeling effect is discussed in section 5. Key findings are summarized in section 6.

2. Model description and experimental design

The fifth-generation Penn State University–National Center for Atmospheric Research (NCAR) Mesoscale Model (MM5, version 3.7.3; Anthes and Warner 1978; Anthes et al. 1987; Grell et al. 1994) is employed to conduct a set of numerical simulations with sophisticated physical processes and nonhydrostatic dynamics. The numerical settings are as in Huang et al. (2011), except for the design of grids points and vertical layers. The horizontal grid spacing of the three nest domains is 27, 9, and 3 km with 337×427, 223×259, and 241×460 grid points, respectively, and the corresponding resolution of the terrain and land-use data is 19, 9, and 4 km. The large outermost domain is used to minimize the effects of fluctuations and disturbances at the lateral boundary on the simulated vortex. There are 23 vertical layers applied to the numerical simulations from the surface to 10 hPa in the terrain-following σ coordinates (σ = 0.995, 0.985, 0.97, 0.945, 0.91, 0.875, 0.825, 0.775, 0.725, 0.675, 0.625, 0.575, 0.525, 0.475, 0.425, 0.375, 0.325, 0.275, 0.225, 0.175, 0.125, 0.075, 0.025). To exclude the impact of the beta effect on the typhoon track, all of the numerical experiments are simulated on f plane located at 15°N. The simple ice scheme of Dudhia (1989) is utilized in the two inner meshes, with the Grell cumulus parameterization (Grell et al. 1994) employed in the outer most mesh. The simple longwave radiation cooling scheme and the high-resolution Blackadar planetary boundary layer (PBL) scheme (Blackadar 1976, 1979; Zhang and Anthes 1982) are applied to all meshes.

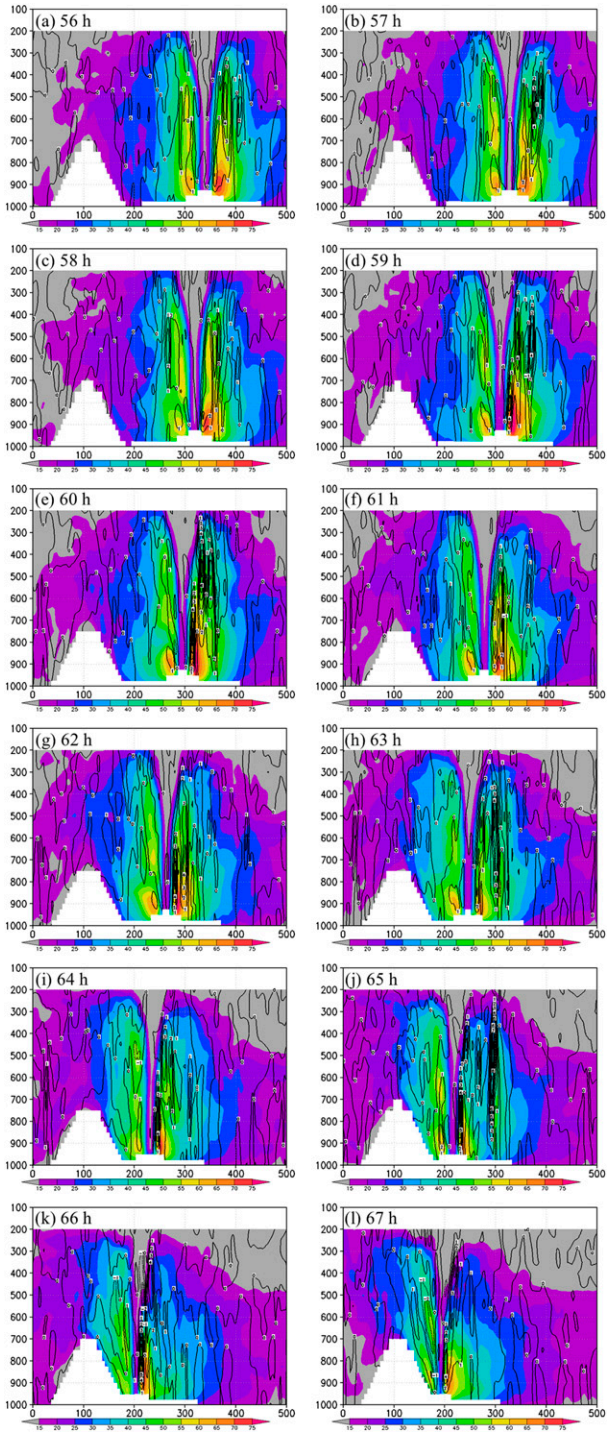

FIG. 4. Vertical cross sections of the meridional wind (shading; m s^{-1}) and the vertical velocity (contours; m s^{-1}) in CTL. The values are averaged from 10 km to the south to 10 km to the north of the TC center (the southward deflection in CTL is identified from 62 to 71 h). The white area on the left is terrain, and the smaller white area on the right is the TC center (no data at several lowest levels owing to the TC's lower surface pressure).

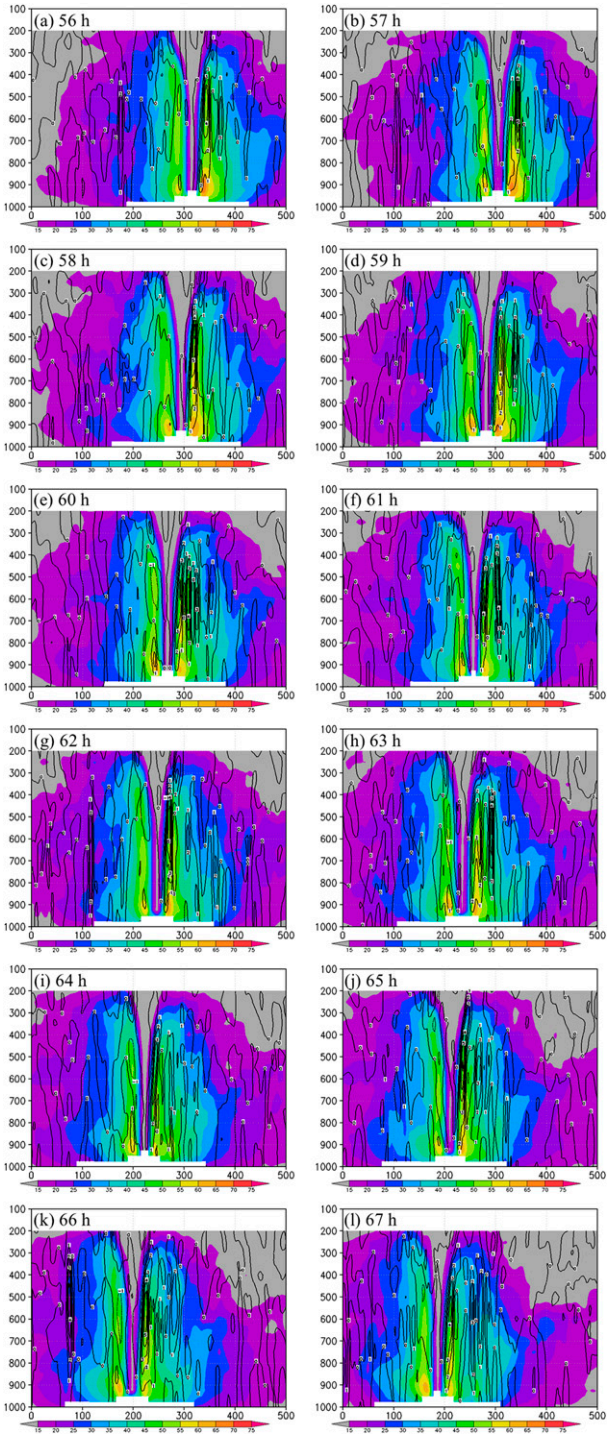

FIG. 5. As in Fig. 4, but for OC-CTL.

Based on the above numerical setting, each simulation is run for 168 h to assess how a typhoonlike vortex responds when impeded by a mesoscale high topography under different flow regimes and topographic properties. First, the control and ocean control experiments are

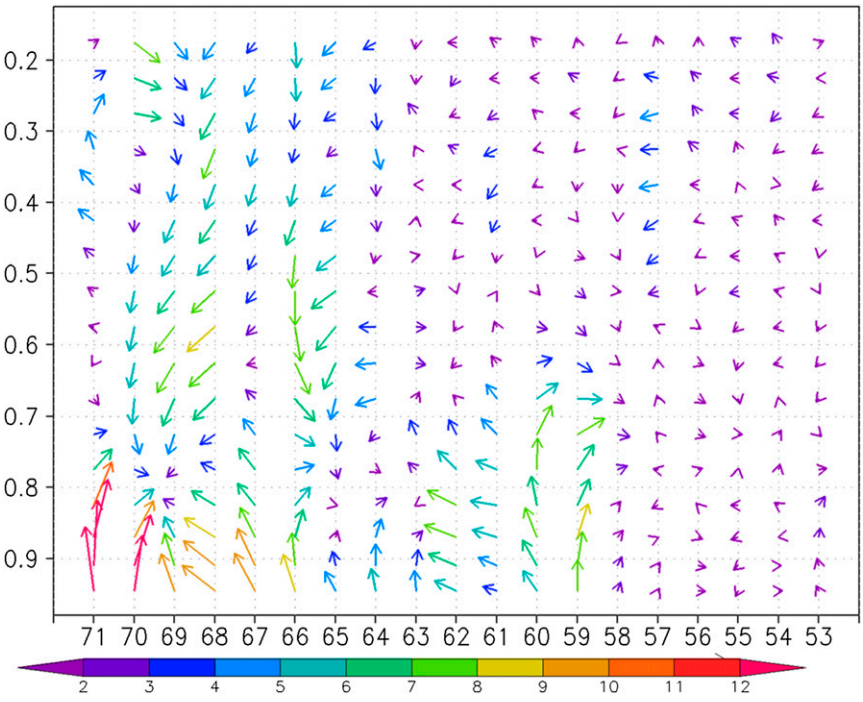

FIG. 6. Difference of the area-mean asymmetric flow (see color bar for magnitude) between CTL and OC-CTL. The difference is obtained by subtracting the results of OC-CTL from CTL. The area-mean value is calculated within the area of a 50-km radius around the TC center. The y axis shows the σ coordinate, and the x axis presents the integration time (h).

conducted with moderate background flow. The idealized Taiwan-like topography is placed in the control experiment, while terrain is excluded and the ocean surface property is used for the ocean control experiment. Second, a set of sensitivity experiments with different flow and/or topographic parameters are performed.

a. Control experiment

Uniform easterly flow at $5\,\mathrm{m\,s^{-1}}$ is used as the basic flow in the control (CTL) and ocean control (OC-CTL) experiments. An idealized vortex structure (DeMaria and Chan 1984) is adopted for the initial vortex structure, prescribed as

$$V' = V_{\max}\frac{r}{r_{\max}}\exp(1/b)[1-(r/r_{\max})^b], \qquad (1)$$

where $V_{\max}$ is the maximum tangential wind speed, $r_{\max}$ is the radius of maximum wind (RMW), and b is a factor that determines the exponential decay rate of the tangential wind beyond $r_{\max}$. We specify $V_{\max} = 35\,\mathrm{m\,s^{-1}}$, $r_{\max} = 50\,\mathrm{km}$, and $b = 0.5$ [as in the idealized setting of Huang et al. (2011)] to construct a vortex representing an intense tropical cyclone with a pertinent structure. The mass field and wind field are balanced following the nonlinear balance equation (Charney 1955). The mean West Indies sounding data from July to October presented in Jordan (1958, their Table 5) are utilized as the reference state for the

TABLE 2. Flow and terrain parameters in each experiment ($f = 3.76\times10^{-5}\,\mathrm{s^{-1}}$, $N = 0.01\,\mathrm{s^{-1}}$). Note that the maximum wind could be located at slightly different altitudes in different experiments.

Experiment	$V_{\max}$ ($\mathrm{m\,s^{-1}}$)	U ($\mathrm{m\,s^{-1}}$)	R (km)	h (m)	L_x (km)	L_y (km)
CTL	78	3.6	36	3000	150	400
H10	78	3.6	36	1000	150	400
H50	78	3.6	36	5000	150	400
A75	78	3.6	36	3000	75	400
A300	78	3.6	36	3000	300	400
B200	78	3.6	36	3000	150	200
B600	78	3.6	36	3000	150	600
$I + 15$	78	3.6	36	3000	150	400
$I - 15$	78	3.6	36	3000	150	400
H2N	78	3.6	36	3000	150	400
H2S	78	3.6	36	3000	150	400
T27	70	3.6	32	3000	150	400
SML	78	3.6	20	3000	150	400
LGE	78	3.6	50	3000	150	400
SLW	78	2.5	36	3000	150	400
MED	78	3.3	36	3000	150	400
FST	78	4.8	36	3000	150	400

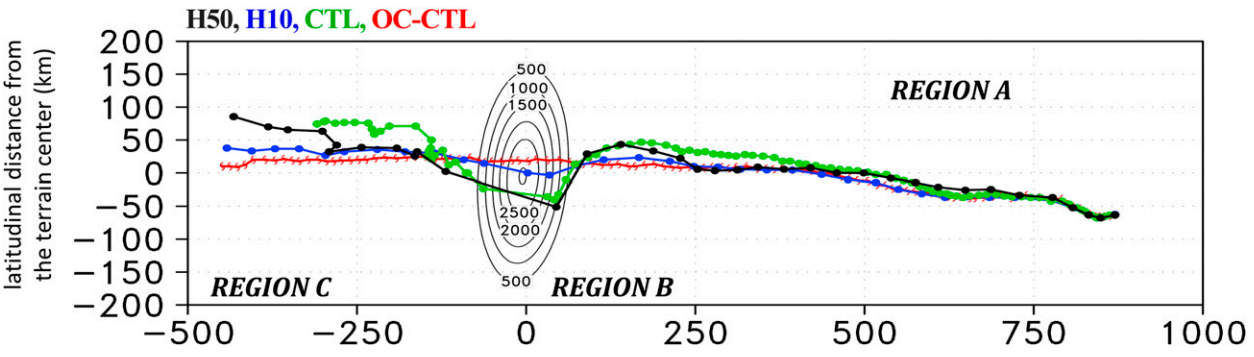

FIG. 7. As in Fig. 1, but for H50 (black) and H10 (blue).

initial fields, including pressure, height, temperature, and relative humidity.

The idealized bell-shaped topography described in Lin et al. (1999) is used in this study:

$$h(x,y) = \frac{h_{\max}}{[(x/a)^2 + (y/b)^2 + 1]^{3/2}}, \quad (2)$$

where h is the mountain height, $h_{\max}$ is the peak value of the mountain height, and a and b indicate the half-width and half-length of the mountain, respectively. To make the edge of the topography zero, as well as to set the terrain center to (longitude, latitude) = (x_c, y_c), we rewrite Eq. (2) as

$$h(x,y) = \frac{h'_{\max}}{\{[(x-x_c)/a]^2 + [(y-y_c)/b]^2 + 1\}^{3/2}} - h', \quad (3)$$

where $h' = h'_{\max}/2^{3/2}$; $h'_{\max}$ is determined by the maximum terrain height, defined as $h'_{\max} = h_{\max}(1 + 1/2^{3/2})$. A family of parameters ($h_{\max}$ = 3 km, a = 75 km, b = 200 km, x_c = 24.0°N, y_c =121.1°E) are used to construct an idealized terrain that mimics the properties of the Taiwan topography. Mixed forest is used to represent the land properties of the mountain topography.

By comparing results between CTL (with the aforementioned bell-shaped terrain) and OC-CTL (solely with the ocean surface), this study examines how a westward-moving vortex responds when approaching the topography. To obtain an initial condition with adjusted model physics, a number of preruns are carried out. First, a simulation is run to spin up the vortex in a quiescent background environment. After 7-day integration, the vortex in this prerun reaches a quasi-steady state, with its maximum wind speed at 0.7-km height and around 70 m s^{-1}, the radius of maximum wind around 60 km, the minimum central sea level pressure at 933 hPa, and the gale-force wind radius around 300 km. Second, two types of preruns are performed for the basic flow (vortex excluded), one embedded with topography and the other with solely the ocean surface. The average flow speed of basic flows in the preruns, either with or without topography, has a steady and moderate magnitude of 3–4 m s^{-1}. In the prerun with basic flow and topography, the basic flow is deflected and split by the terrain. In addition, a clear lee-side vortex is present in this simulation (not shown), in general consistent with the results of previous studies (e.g., Smith and Smith 1995; Smolarkiewicz and Rotunno 1989).

After the above preruns are conducted, the spun-up vortex is embedded in the background flow to construct the idealized simulations. The vortex is placed 800 km east of the terrain. The geographic center of the topography is implanted at 24°N, collocated with the latitudinal position of the vortex center in OC-CTL after the initial adjustment.

b. Sensitivity experiments

A set of experiments is carried out to investigate the sensitivity of TC motion to the height, shape, and range of terrain; the intensity, structure, and latitudinal position of the initial vortex; vortex translation speed; and the angle at which the vortex approaches the topography. Details of the idealized experimental design are provided in Table 1. To demonstrate the sensitivity of TC track to mountain height, experiments with $h_{\max}$ = 5 and 1 km are carried out (H50 and H10 in Table 1). Simulations with the narrower and wider topography are performed with $2a$ = 75 and 300 km in Eq. (3) and are referred to as A75 and A300 (Table 1), respectively. Sensitivity simulations with respect to the topography length ($2b$ = 200 and 600 km for B200 and B600, respectively) are also conducted. Vortex intensity and structure are also altered by using different $V_{\max}$ and $r_{\max}$ values in Eq. (1) for the vortex preruns. A weaker storm is used to assess the sensitivity to a small deviation in the maximum wind for an intense TC (T27 in Table 1). The response of a TC with a smaller or larger RMW to the topography is examined as well (SML and LGE in Table 1). By rotating the terrain and changing

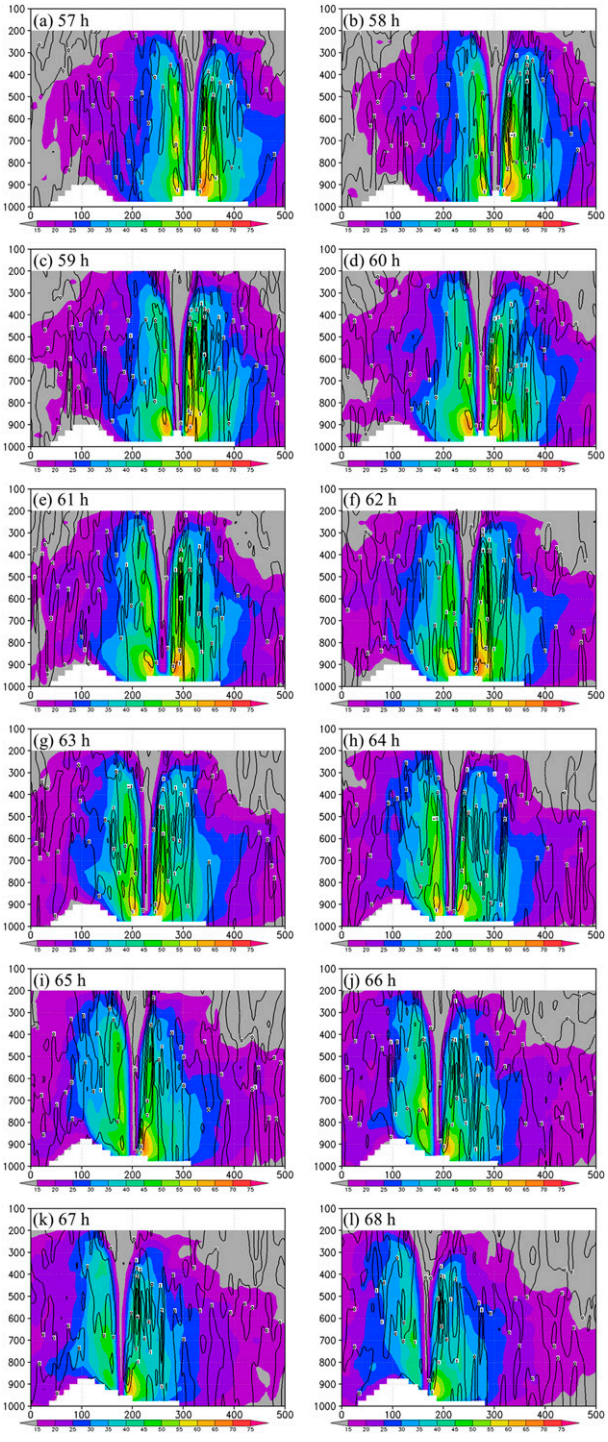

FIG. 8. As in Fig. 4, but for H10 (the southward deflection in H10 is identified from 62 to 71 h).

the mountain's center position, experiments with varying TC incident angle ($I + 15$ and $I - 15$ in Table 1) and initial position are conducted (H2N and H2S in Table 1). Different magnitudes of initial easterly background flow are also adopted in the sensitivity experiments to understand how the TC responds to the topography when traveling at different translation speeds (SLW, MED, and FST in Table 1). The position of the topography center is implanted at different latitude, collocated with the latitudinal position of the vortex center in each corresponding ocean experiment after the initial adjustment.

3. The control experiment

Figure 1 shows the track of the CTL and OC-CTL experiments. During the initial 24 h of the simulation, the storms in both CTL and OC-CTL follow similar west-northwestward tracks, demonstrating that the terrain has little impact on the track of CTL in which the vortex center is more than 600 km upstream of the topography. After 24 h, OC-CTL persistently travels westward, primarily steered by the background easterly flow, until the end of the integration. Meanwhile, the difference of the vortex movement between OC-CTL and CTL appears and becomes distinct after 40 h. From 40 to 60 h, a period when the vortex center is about 200–600 km upstream of the topography (denoted as region A in Fig. 1), CTL is deflected to the north under the influence of the topography. During the later hours, sometime between 62 and 71 h, a period just before and during the storm center's passage through the mountain, the TC movement in CTL experiences a sudden change from west-northwestward to southwestward. The spatial interval where the southward deflection of CTL occurs is denoted as region B (Fig. 1). The southward deflection of CTL is about 100 km, which is measured from the northernmost extent to the southernmost extent of the TC track in region B. When the vortex center of CTL is about to leave the topography ($t = 72$ h), CTL storm makes a pronounced northward turn again. The region in which CTL moves northward after 72 h is denoted as region C. The corresponding mechanisms of track deflections in CTL in regions A, B, and C are investigated in this section.

The representativeness of using steering flow for the vortex motion (Chan and Gray 1982; Wu and Emanuel 1995a,b) is examined. The deep = layer areal (σ = 0.825–0.325)-mean asymmetric flow in an area of $1° \times 1°$ around the storm center is calculated as the steering flow for TC movement in this study.[2] It is found that the

[2] The steering flow concept regards the tropical cyclone as a rigid vortex (or simply a point vortex) advected by the mean environmental flow crossing the storm center. The calculation within a small area with high-spatial-resolution data can well represent the steering flow (Roux and Marks 1991; Wu and Emanuel 1995a,b).

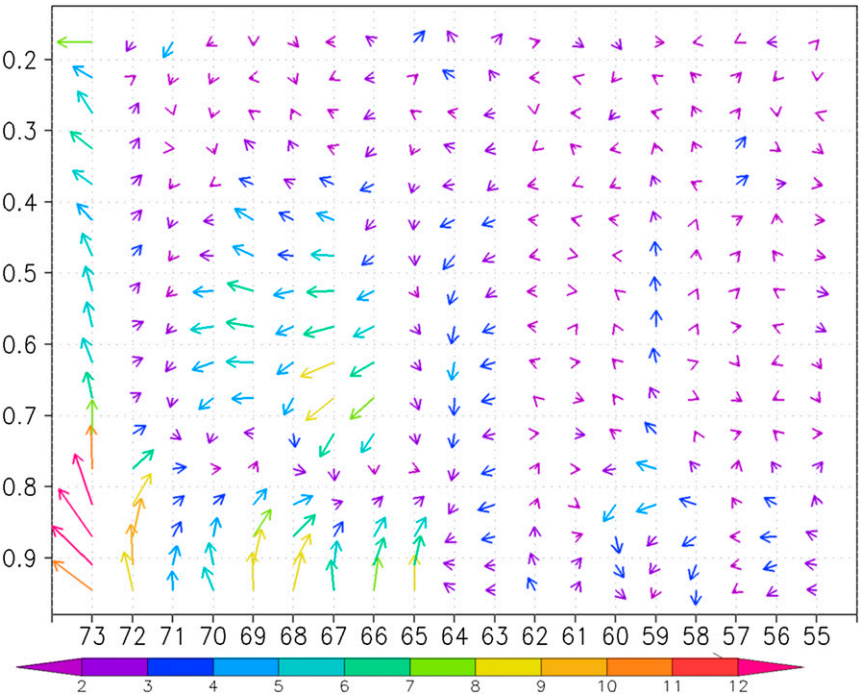

FIG. 9. As in Fig. 6, but for H10. The difference is obtained by subtracting the results of OC-CTL from H10.

direction indicated by the evaluated steering-flow vector mostly aligns with the TC motion vector in both regions A and B (cf. Figs. 1 and 2), despite some deviations in magnitude and direction found prior to landfall (with one exception of large discrepancy at 66 h; Fig. 2b). In region C, the storm is much weaker and less organized after passing over the mountain and, thus, is farther away from being a rigid or stiff vortex. This may cause the vortex to deviate from the steering flow (Fig. 2). In Huang et al. (2011; their Fig. 13), it was shown that the northwestward movement of the storm in region C can be explained by the channeling winds between the topography and the eastern side of the storm as well. Wind enhancement in the channel is also found in this study (figures not shown) as the storm is leaving the topography. The concurrently induced northward component of the deep-layer-mean flow may thus serve as a possible explanation for the northwestward movement during this time period. However, uncertainties over locating a weaker and loose circulation may grow, causing higher uncertainties in obtaining storm-motion vectors and steering flow in region C. Therefore, this study intends to focus the discussion on changes in TC track prior to landfall, when the storm center can be well defined.

According to the alignment of TC motion vectors and the obtained asymmetric flow, one may infer that understanding the dynamical process causing the asymmetric flow is very likely to provide valuable insights into the mechanism(s) responsible for changes in the storm's movement in regions A and B. The northward (southward) deflection in region A (region B) corresponds to the northward (southward) deflection of the evaluated steering flow, consistent with results of Lin and Savage (2011) and Jian and Wu (2008). While the northward steering flow in region A is found closely connected to the terrain-induced deflection of the basic easterly flow (i.e., the topographic effect on the large-scale flow, and thus on the TC movement), the identified steering flow in region B is different from the terrain-deflected basic flow (figures not shown). The northerly steering flow such as that obtained in region B was shown to be related to the channeling effect (the terrain-induced effect on the vortex structure) in Jian and Wu (2008) and Huang et al. (2011). In these two previous studies, enhanced northerly low-level jet was found to the west of the storm center and was attributed to the enhancement of the low-level cyclonic TC circulation in the narrow region between the storm center and the high topography. The role of the channeling effect on the southward deflection in region B in CTL is thus investigated in this study.

As in the previous studies (e.g., Jian and Wu 2008; Huang et al. 2011), the backward trajectory analysis of

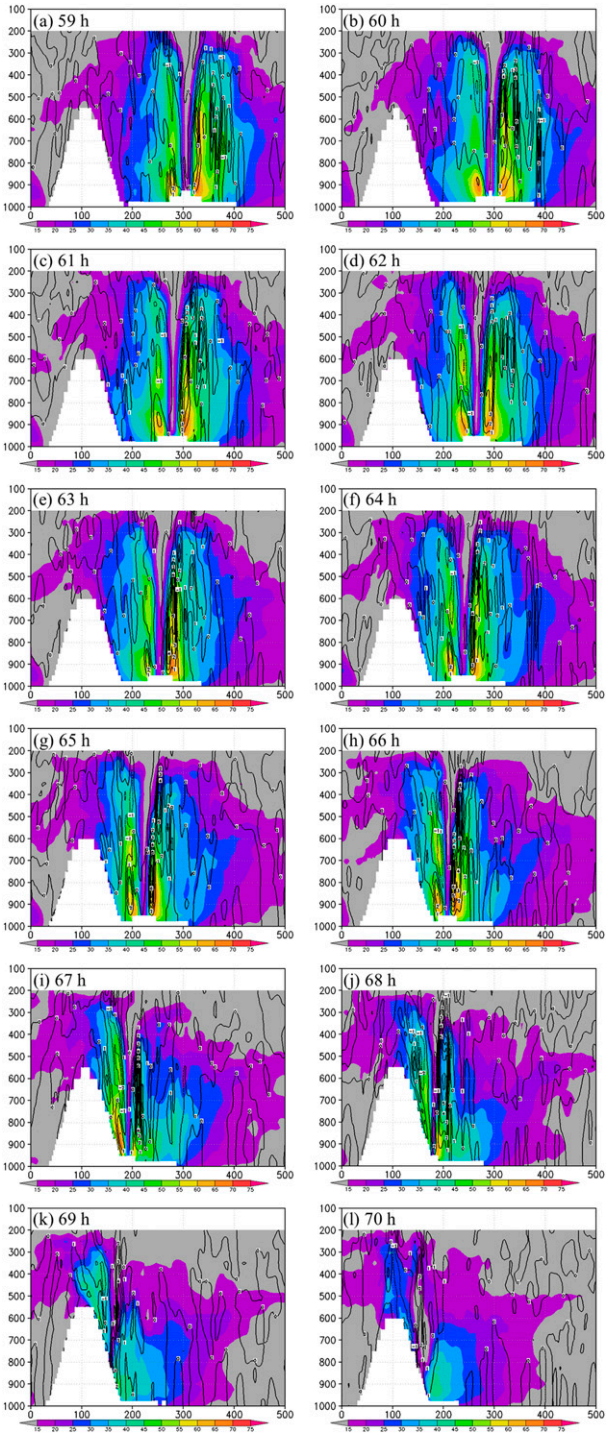

FIG. 10. As in Fig. 4, but for H50 (the southward deflection in H50 is identified from 66 to 71 h).

air parcels is used to examine the occurrence of the channeling effect during the storm's southward deflection. Unlike the parallel trajectories obtained in OC-CTL, the air parcels in CTL become slightly confluent when passing through the channel between the topography and the storm center (Fig. 3). Nevertheless, the identified small confluence does not produce a distinct northerly low-level jet (cf. Figs. 4 and 5) as pointed out in Jian and Wu (2008) and Huang et al. (2011). The absence of the low-level northerly jet west to the TC center demonstrates that channeling effect is not the mechanism causing the southward deflection of the storm in CTL. Instead, Fig. 4 shows changes in the midtropospheric winds (roughly between 700 and 300 hPa). Before 60 h, the midtropospheric winds on eastern and western sides of the TC have similar strength. A transient vertically upward extension of the wind maximum in the eastern eyewall occurs at 61 and 62 h and enhances midtropospheric winds east to the storm center. After 62 h, when the storm in CTL starts to make a southward turn, the enhancement or maintenance of winds on the western side of the storm, together with a continual decrease in wind speeds east to the TC center, generating asymmetry of midtropospheric winds. This asymmetry of midtroposphere wind speeds around the storm center grows as the storm moves toward the terrain, in agreement with the increasing southward deflection of the TC track (cf. Figs. 1 and 4g–l). The elevations where the northerly asymmetric flow occurs are apparently different from those shown in Jian and Wu (2008) and Huang et al. (2011). The result of CTL suggests a different dynamical pathway of the terrain-induced southward TC track deflection.

The difference in the areal-mean asymmetric-flow vector between CTL and OC-CTL (Fig. 6) further demonstrates that the northerly steering flow at the middle level (σ = 0.7–0.3, around 2.7–7 km) between 65 and 70 h (corresponding to region B in Figs. 1 and 2) reflects the steering flow for the southward-moving storm in CTL. It is the combined effect of the terrain-induced strengthening wind on the western side of the TC, which either enhances or maintains the winds, and the terrain-induced reduction in wind speeds on the eastern side of the TC in the midtroposphere that contributes to the northerly deep-layer-mean steering flow, resulting in the southward deflection of the TC in region B (cf. Figs. 1, 2, 4, and 6).

4. Sensitivity experiments

Sensitivity experiments are performed with different parameters describing the structure of the idealized vortex and topography. Simulations showing greater variability are discussed in this section, including those with different mountain heights, TC incident angles, initial positions, intensities, and translation speeds (see Tables 1 and 2).

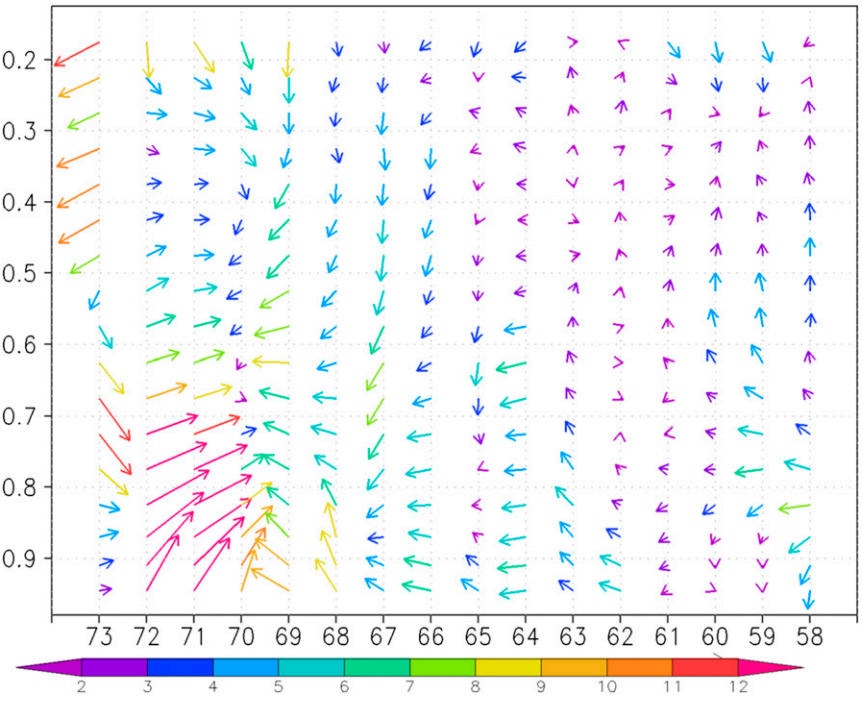

FIG. 11. As in Fig. 6, but for H50. The difference is obtained by subtracting the results of OC-CTL from H50.

a. Influence of mountain height

In addition to CTL, which has the terrain maximum height at 3000 m, two experiments with the maximum mountain heights of 5000 m (H50) and 1000 m (H10) are conducted to understand the impact of mountain height on TC movement. Compared with the magnitude of the track deflection in CTL, H50 shows similar southward deflection to CTL, while in H10 the deflection is apparently reduced (Fig. 7). Although CTL and H10 show that the terrain-induced track deflection is larger for an intense TC encountering a higher mountain, CTL and H50 demonstrate the convergence behavior of the southward deflection. These results are not inconsistent with the findings of Lin et al. (2005), which showed that the smaller Fr is, the larger the TC deflection could be.

Changes in the vortex structure of H10 and H50 are also analyzed to examine the close connection between the TC's southward track deflection and asymmetric winds as demonstrated by the result of CTL. Similar to CTL, during the storm's southward turn in H10, enhanced winds at low levels (the product of the channeling effect) on the western side of the TC are absent (cf. Figs. 4 and 8), and the azimuthal asymmetry of tangential winds at middle levels is evident (Figs. 8f–j). This result further supports the mechanism proposed based on CTL. Since the difference in wind speeds between the western and eastern sides at the midlevel is smaller than that in CTL, the consequential deep-layer-mean northerly steering flow is smaller (Fig. 9), and thus the magnitude of the TC's southward deflection is nearly absent in H10 (Fig. 7).

As in CTL and H10, the signal of low-level northerly jet induced by the channeling effect is unclear on the western side of the TC in H50. Only limited enhancement of wind speed in the channel is found between 59 and 60 h (Figs. 10a,b) and between 66 and 67 h (Figs. 10h,i). During 60–66 h, wind speeds on the western side of the TC remain unchanged when the storm is approaching the topography. The asymmetric flow further demonstrates that even though the channeling effect may contribute to the maintenance or slight increase in wind speeds, its impact is apparently insufficient to generate low-level northerly asymmetric flow to drift the TC southward (Fig. 11). In contrast, the asymmetric wind at the midtroposphere (Fig. 11), which is used to explain the storm's southward track deflection for CTL and H10, is also present in H50. Comparisons among the results of CTL, H10, and H50 indicate the robust role of the midtropospheric northerly asymmetric flow in the storm's southward deflection. Results of CTL and H10 imply that the strength of such asymmetric flow is highly

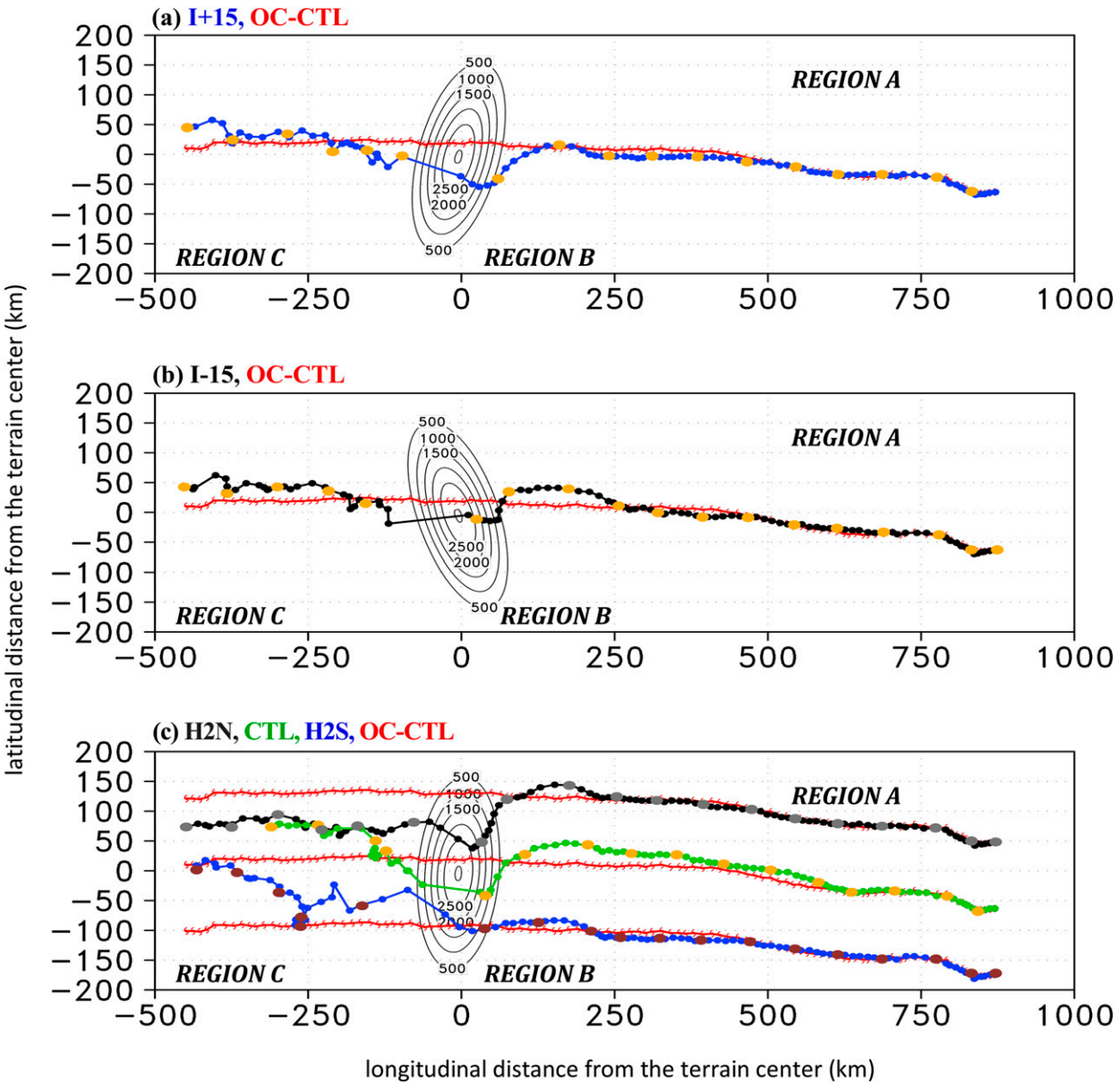

FIG. 12. As in Fig. 1, but for (a) $I + 15$ (blue), (b) $I - 15$ (black), and (c) H2N (black) and H2S (blue). Results of the corresponding ocean control experiments are in red.

related to the terrain height—a higher terrain induces more pronounced asymmetric flow (cf. Figs. 6 and 9), while steering flows in CTL and H50 (cf. Figs. 6 and 11) share much similarity.

b. *Sensitivity to TC incident angle and TC initial position*

By horizontally rotating the idealized terrain, another group of sensitivity experiments is conducted to investigate the impact of the storm's incident angles (Figs. 12a,b). Compared with CTL (also shown in Fig. 12c; 100 km southward if it is measured from the northernmost point to the southernmost point), both $I + 15$ (rotating the terrain clockwise by 15°) and $I - 15$ (rotating the terrain counterclockwise by 15°) show less significant southward deflection (60- and 50-km southward deflection, respectively) prior to landfall. Before making this southward turn, however, the direction of the TC motion in $I + 15$ does not undergo a distinct northward turn as found in other simulations (e.g., CTL, H10, H50, and $I - 15$). The different tracks in these two experiments demonstrate that the

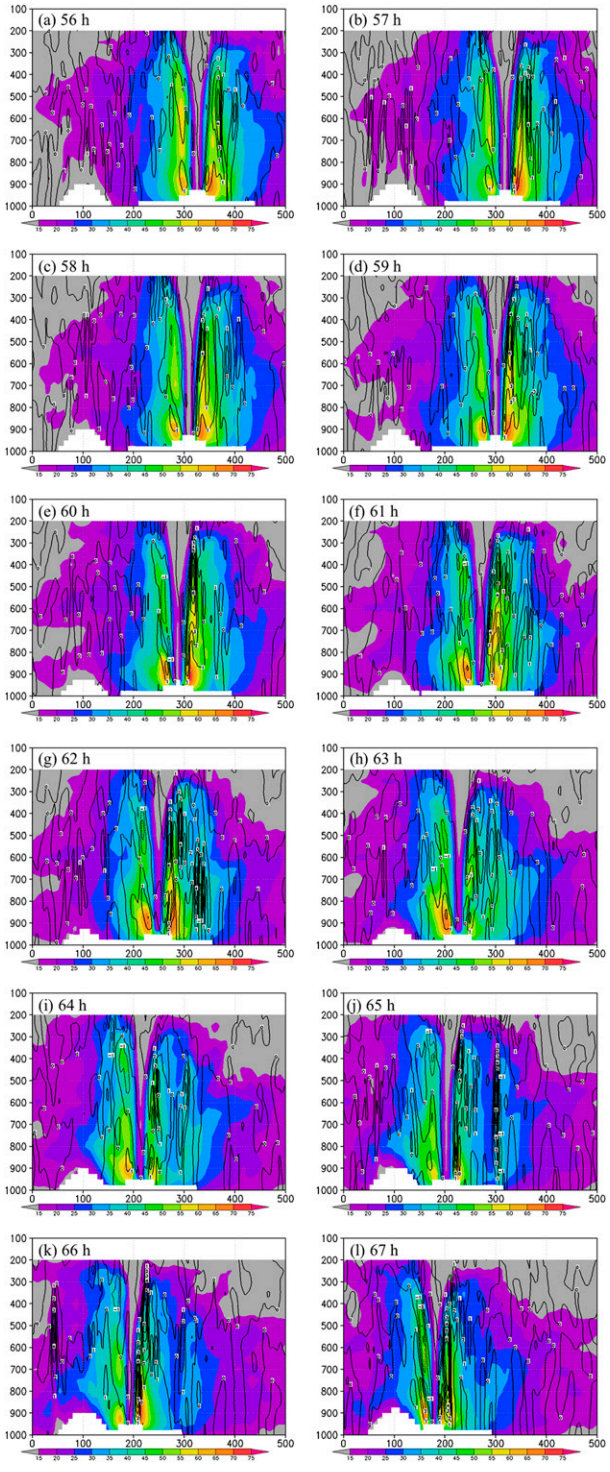

FIG. 13. As in Fig. 4, but for H2N (the southward deflection in H2N is identified from 61 to 74 h).

incident angle could affect the TC track deflection, especially in region A.

Furthermore, experiments H2N and H2S are performed to understand how the vortex responds when approaching different portions of the topography. The initial vortex in H2N (H2S) is embedded in the basic flow 1° latitude to the north (south) of the CTL vortex. Compared with CTL (with 100 km southward in region B), southward deflection of the TC track is slightly greater in H2N (at 110 km southward) but much less in H2S (roughly 30 km) (Fig. 12c). This finding demonstrates that as the storm moves toward the northern and central portion of the topography, it may undergo more pronounced southward track deflection, consistent with findings of Huang et al. (2011). Stronger wind speed at low levels (the product of the channeling effect) on the western side of the TC is identified in H2N during the early stage of the storm's southward turn (61–64 h; Figs. 13f–i). Figure 14 shows that corresponding southward asymmetric flow starts to appear at low levels (below $\sigma = 0.85$) around 60 h and weakens after 64 h. The asymmetric flow is also present at higher levels after 63 h, suggesting the occurrence of low-level and midtropospheric northerly jets together contribute to drift the TC southward in H2N.

c. *Sensitivity to TC intensity and TC translation speed*

Sensitivities to TC intensity and TC translation speed are examined in this section. In an experiment with a weaker vortex (V_{max} is 8 m s^{-1} weaker than CTL; see T27 in Tables 1 and 2 for details), the storm experiences similar southward deflection (100 km) near the topography (Fig. 15a) to that in CTL. This suggests that the terrain-induced southward deflection is not sensitive to such a deviation in V_{max} of intense TCs embedded in the moderate basic flow. The impacts of topography on TC tracks at different TC translation speeds are obtained by embedding the vortex in basic flow with different speed (Figs. 15b–d). The TC translation speed in SLW (slower basic flow; Fig. 15b), MED (medium basic flow; Fig. 15c), and FST (faster basic flow; Fig. 15d) are 2.5, 3.3, and 4.9 m s^{-1}, respectively. Among these three simulations, slower TC movement (i.e., a smaller Fr of the basic flow) leads to more southward deflection near the topography. This is consistent with results of Lin et al. (2005) and other previous studies, although this study mainly focuses on the flow regimes for intense typhoons.

5. Impact of channeling effect

According to the results of CTL and a series of sensitivity experiments, the acceleration of low-level winds is not the universal feature for TCs experiencing southward track deflection near the topography. Our

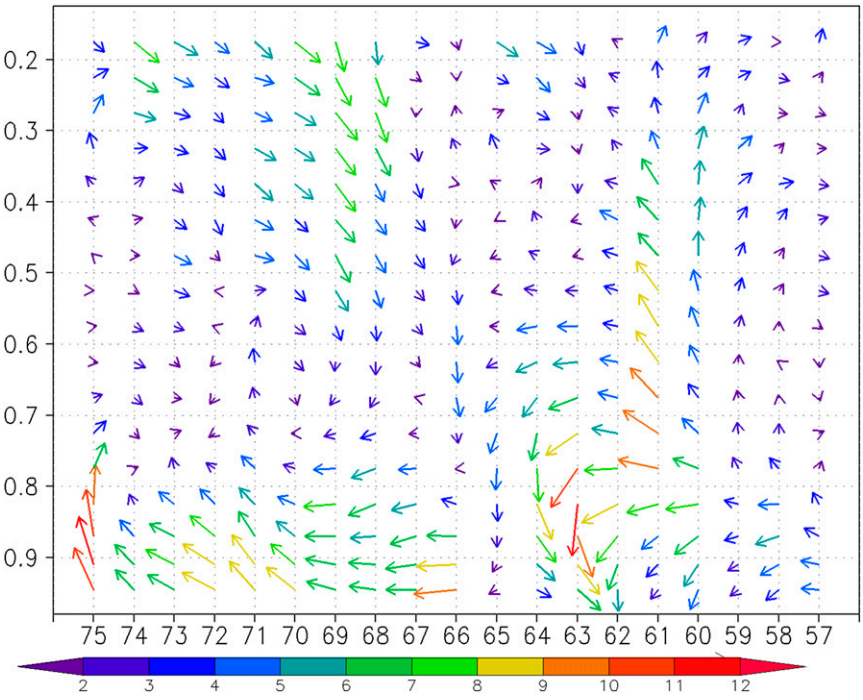

FIG. 14. As in Fig. 6, but for H2N. The difference is obtained by subtracting the results of OC-CTL from H2N.

new findings suggest that the conventional channeling effect is not a robust flow characteristic and, thus, cannot serve as the dominant dynamical pathway leading to the southward TC movement near topography. Low-level winds enhanced to the west of the storm are solely found in H2N (a vortex approaching the northern portion of topography) during the first few hours of the TC's southward turn, suggesting a supporting impact of channeling effect on the TC's southward movement. The backward trajectory analysis shows that air parcels in H2N are obviously affected by the terrain and become confluent when passing the channel between the storm center and topography, while those in CTL start to converge at the northwestern side of the storm (Fig. 16). It is speculated that the broader space to the north of the storm in H2N may allow more air parcels to enter the channel between the storm center and topography and, thus, may contribute to the stronger confluent flow and channeling winds at lower levels. In conclusion, the channeling effect that results in the low-level northerly jet seems to occur for an intense TC approaching the northern topography while being absent or unclear in the remainder of the simulations. In addition, channeling-effect-induced low-level wind acceleration plays a supporting role in leading to the southward turn of the storm in H2N.

6. Concluding remarks and issues to be further addressed

While the northward track deflection has been documented in some earlier studies (Brand and Blelloch 1974; Wang 1980; Chang 1982; Bender et al. 1987; Yeh and Elsberry 1993; Wu 2001) for TCs approaching Taiwan topography from the east, a number of recent studies (Jian and Wu 2008; Huang et al. 2011) have pointed out that an intense typhoon may occasionally make a sudden southward turn just prior to and during the landfall. As a follow-up study of Huang et al. (2011), this work investigates more flow and parameter regimes to further understand the impact of mesoscale topography on TC movement and the role of the channeling effect in the sudden southward turn of a TC vortex. An important finding of this work is that the robust flow characteristic identified during the southward turn of a TC is the azimuthal asymmetry of tangential winds at middle levels, not the asymmetry caused by channeling winds at lower levels. To examine whether the vertical resolution would affect the result, we carry out an additional experiment with 32 vertical levels, as in Huang et al. (2011). The result of this experiment agrees well with the findings presented in this study, supporting the finding of a different mechanism for the terrain-induced southward track deflection as compared with Huang

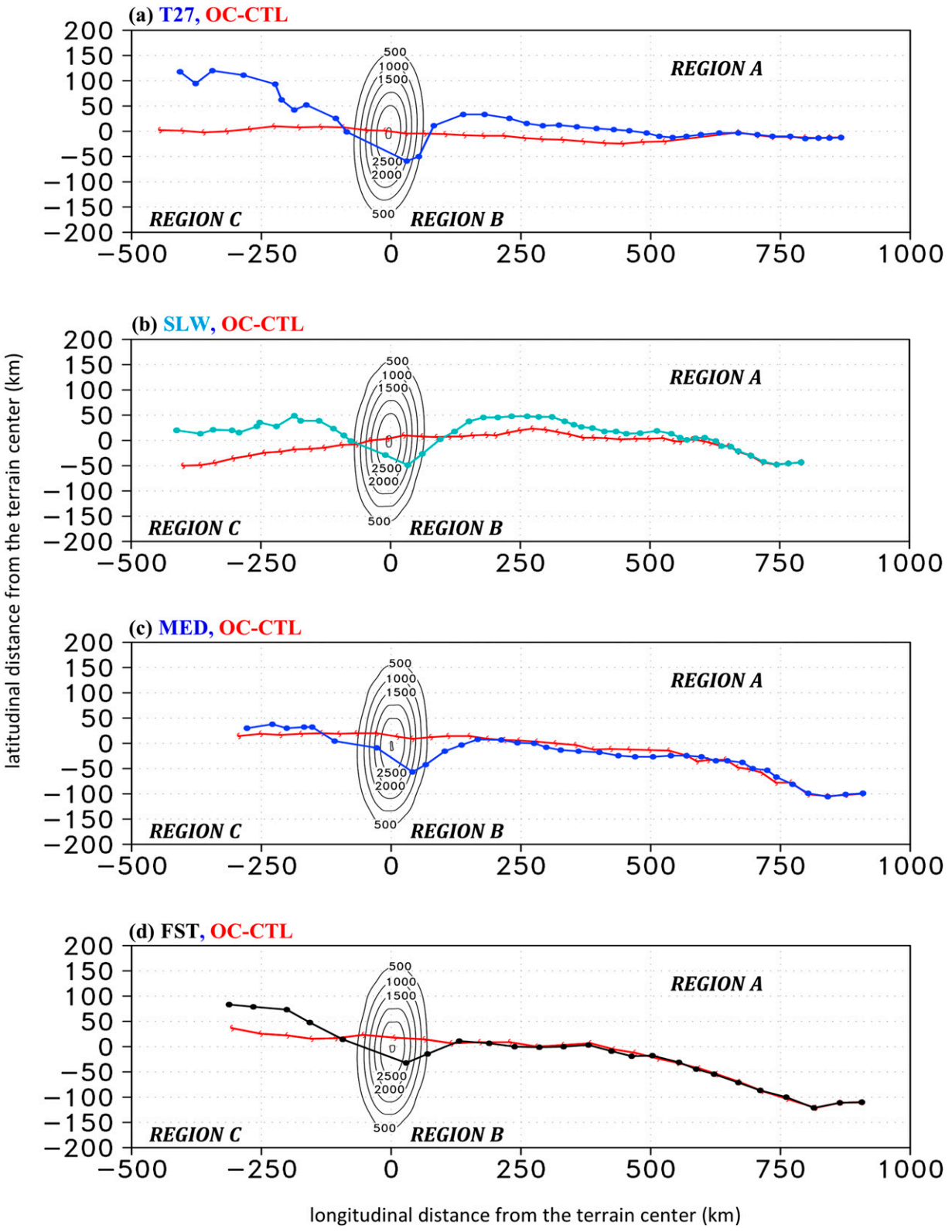

FIG. 15. As in Fig. 1, except showing the TC track of (a) T27, (b) SLW, (c) MED, and (d) FST. Results of the corresponding ocean control experiments are in red. TC centers are marked by either a closed circle or a typhoon symbol every 3 h.

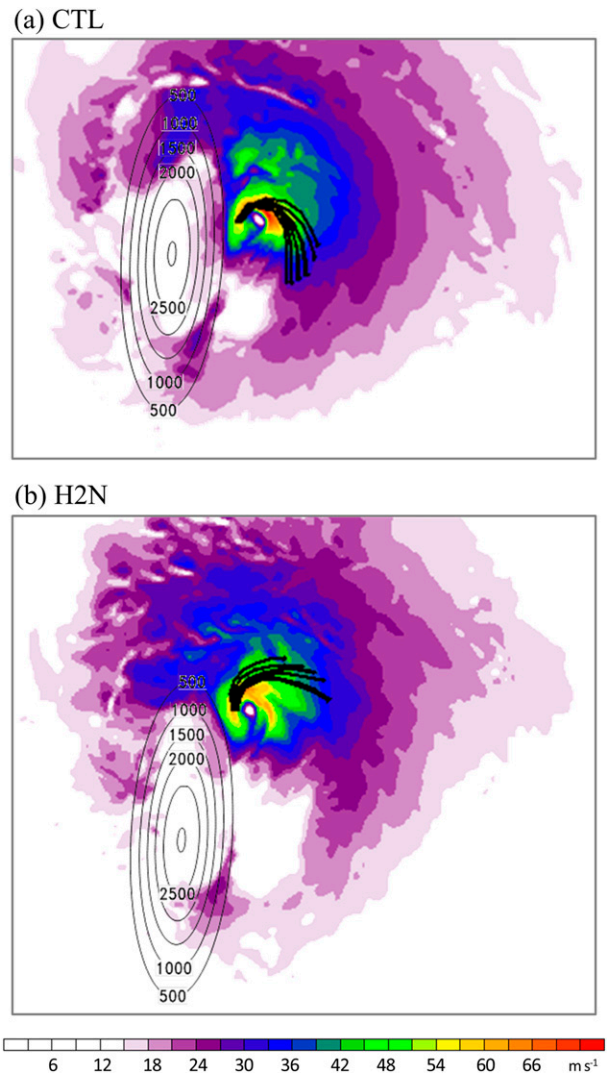

FIG. 16. As in Fig. 3, but for (a) CTL and (b) H2N at 66 h.

et al. (2011). The midlevel winds that weaken to the east and strengthen/remain unchanged to the west of the TC center in the vortex's inner core are considered responsible for enhancing the northerly steering flow that advects the TC southward near the topography. Moreover, the azimuthal changes in the winds speeds appear to be connected to the changes in the vertical velocity, suggesting the importance in further examining the relationship between the terrain-induced changes in both primary and secondary circulations. The momentum budget analysis is yet to be carried out to fully understand the dynamical processes leading to the weakening (enhancement/maintenance) of winds east (west) of the TC center during the storm's southward deflection. Meanwhile, the asymmetry of water vapor mixing ratio and potential stability is examined. A region of a drier and relatively stable air is found east to the storm center at low and middle levels (figures not shown). This implies that terrain-induced azimuthal changes in the thermodynamic structure of a TC (e.g., changes in diabatic heating and the atmospheric static stability) and its connection to the asymmetry of midlevel tangential winds need to be further explored, as the thermodynamic structure is closely related to the changes of the overturning circulation and thus to the TC's primary circulation.

In the sensitivity experiments, examinations are conducted with respect to different parameters describing the idealized vortex and mountain, including the mountain height, width, and length, as well as the incident angle, initial position, intensity, the radius of the maximum wind, and translation speed of the TC. The result demonstrates that the southward track deflection prior to landfall is a common phenomenon among intense TCs under various flow regimes. Findings further point out that intense TCs experience greater southward deflection prior to landfall when the mountain is higher, when the vortex approaches the northern and middle portion of the terrain, or when the storm moves slower. In addition to the results presented in section 4, limited variability is found among sensitivity experiments to the mountain width (narrower: A75; wider: A300) and length (shorter: B300; longer: B600), as well as the storm's RMW (SML: smaller; LGE: larger) under the flow regimes of an intense TC and moderate basic flow (Fig. 17 and Tables 1–3). The R/L_y values adopted in this study are relatively small (from 0.09 to 0.15) and in the regime where vortices were anticipated to make a southward turn near topography in Lin et al. (2005). According to findings in Lin et al. (2005), one might expect that a TC with a realistic RMW (10–150 km; Willoughby and Rahn 2004; Kossin et al. 2007), corresponding to the small value of R/L_y, would experience southward track deflection when approaching a terrain similar to that of Taiwan. Although the coherent southward deflection of TC motion in this study (e.g., Figs. 17e,f) shows supporting evidence, it should be noted that other factors may also need to be evaluated. First, microphysics and surface processes, which are not included in the numerical experiments of Lin et al. (2005) but are important in the evolution of a TC in the real world, are likely to impact interactions among the terrain, environmental flow, and TC and thus can influence the terrain-induced changes in TC structure and motion. Second, it is still unclear how a TC at moderate or weak intensity responds to terrain in different flow regimes since only intense TCs are investigated in the current study. These issues require

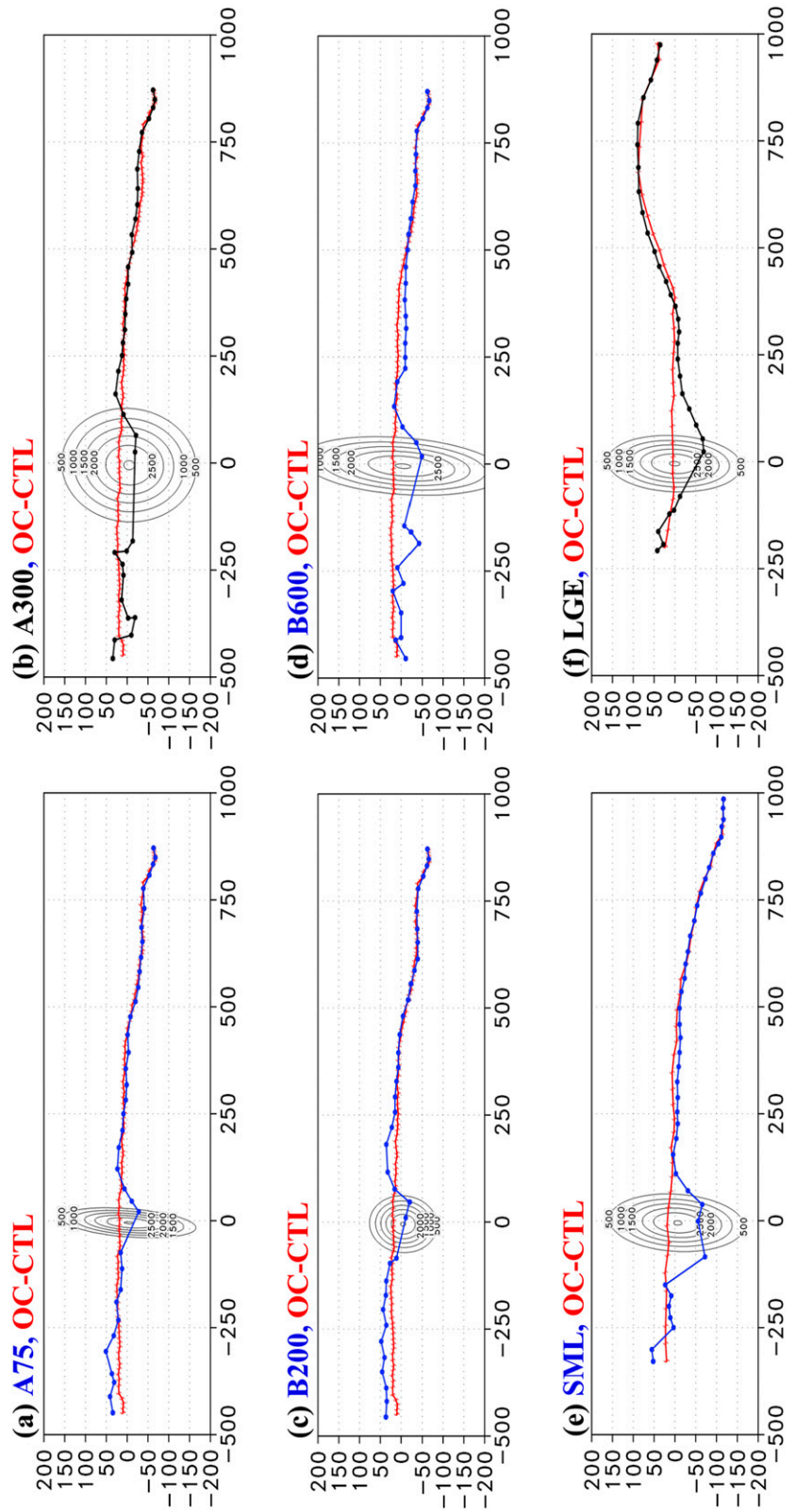

FIG. 17. As in Fig. 15, but for (a) A75, (b) A300, (c) B200, (d) B600, (e) SML, and LGE.

TABLE 3. The nondimensional parameters in each experiment ($f = 3.76 \times 10^{-5}\ s^{-1}$, $N = 0.01\ s^{-1}$).

Experiment	V_{max}/Nh	U/Nh	R/L_y	U/fL_x	V_{max}/fR	h/L_x
CTL	2.6	0.12	0.09	0.62	59.3	0.02
H10	7.8	0.35	0.09	0.62	59.3	0.0067
H50	1.56	0.07	0.09	0.62	59.3	0.033
A75	2.6	0.12	0.09	1.24	59.3	0.04
A300	2.6	0.12	0.09	0.31	59.3	0.01
B200	2.6	0.12	0.15	0.62	59.3	0.02
B600	2.6	0.12	0.05	0.62	59.3	0.02
$I + 15$	2.6	0.12	0.09	0.62	59.3	0.02
$I - 15$	2.6	0.12	0.09	0.62	59.3	0.02
H2N	2.6	0.12	0.09	0.62	59.3	0.02
H2S	2.6	0.12	0.09	0.62	59.3	0.02
T27	2.33	0.12	0.08	0.62	58.1	0.02
SML	2.26	0.12	0.05	0.62	90.4	0.02
LGE	2.26	0.12	0.125	0.62	36.1	0.02
SLW	2.6	0.083	0.09	0.44	59.3	0.02
MED	2.6	0.11	0.09	0.59	59.3	0.02
FST	2.6	0.16	0.09	0.69	59.3	0.02

further examination. In all, this study highlights the robust asymmetric flow in the midtroposphere as a new mechanism other than the traditional channeling effect that contributes to the terrain-induced southward track deflection.

Acknowledgments. The authors thank Dr. Yuh-Lang Lin and two other reviewers for providing valuable comments. The authors of this paper are supported by the National Science Council of Taiwan under Grants NSC 102-2628-M-002-008 and 101-2111-M-002-008-MY3.

REFERENCES

Anthes, R. A., and T. T. Warner, 1978: Development of hydrodynamic models suitable for air pollution and other mesometerological studies. *Mon. Wea. Rev.,* **106,** 1045–1078, doi:10.1175/1520-0493(1978)106<1045:DOHMSF>2.0.CO;2.

——, E.-Y. Hsie, and Y.-H. Kuo, 1987: Description of the Penn State/NCAR Mesoscale Model Version 4 (MM4). NCAR Tech. Note NCAR/TN-282+STR, 66 pp.

Bender, M. A., R. E. Tuleya, and Y. Kurihara, 1987: A numerical study of the effect of island terrain on tropical cyclones. *Mon. Wea. Rev.,* **115,** 130–155, doi:10.1175/1520-0493(1987)115<0130:ANSOTE>2.0.CO;2.

Blackadar, A. K., 1976: Modeling the nocturnal boundary layer. Preprints, *Third Symp. on Atmospheric Turbulence and Air Quality,* Raleigh, NC, Amer. Meteor. Soc., 46–49.

——, 1979: High resolution models of the planetary boundary layer. *Advances in Environmental Science and Engineering,* J. Pfafflin and E. Ziegler, Eds., Vol. 1, Gordon and Breach, 50–85.

Brand, S., and J. W. Blelloch, 1974: Changes in the characteristics of typhoons crossing the island of Taiwan. *Mon. Wea. Rev.,* **102,** 708–713, doi:10.1175/1520-0493(1974)102<0708:CITCOT>2.0.CO;2.

Chan, J. C. L., and W. M. Gray, 1982: Tropical cyclone movement and surrounding flow relationships. *Mon. Wea. Rev.,* **110,** 1354–1374, doi:10.1175/1520-0493(1982)110<1354:TCMASF>2.0.CO;2.

Chang, S. W.-J., 1982: The orographic effects induced by an island mountain range on propagating tropical cyclones. *Mon. Wea. Rev.,* **110,** 1255–1270, doi:10.1175/1520-0493(1982)110<1255:TOEIBA>2.0.CO;2.

Charney, J., 1955: The use of the primitive equations of motion in numerical prediction. *Tellus,* **7,** 22–26, doi:10.1111/j.2153-3490.1955.tb01138.x.

DeMaria, M., and J. C. L. Chan, 1984: Comments on "A numerical study of the interactions between two tropical cyclones." *Mon. Wea. Rev.,* **112,** 1643–1645, doi:10.1175/1520-0493(1984)112<1643:CONSOT>2.0.CO;2.

Dudhia, J., 1989: Numerical study of convection observed during the Winter Monsoon Experiment using a mesoscale two-dimensional model. *J. Atmos. Sci.,* **46,** 3077–3107, doi:10.1175/1520-0469(1989)046<3077:NSOCOD>2.0.CO;2.

Grell, G., J. Dudhia, and D. Stauffer, 1994: A description of the fifth-generation Penn State/NCAR Mesoscale Model (MM5). NCAR Tech. Note NCAR/TN-198+STR, 117 pp.

Hsu, L.-H., H.-C. Kuo, and R. G. Fovell, 2013: On the geographic asymmetry of typhoon translation speed across the mountainous island of Taiwan. *J. Atmos. Sci.,* **70,** 1006–1022, doi:10.1175/JAS-D-12-0173.1.

Huang, Y.-H., C.-C. Wu, and Y. Wang, 2011: The influence of island topography on typhoon track deflection. *Mon. Wea. Rev.,* **139,** 1708–1727, doi:10.1175/2011MWR3560.1.

Jian, G.-J., and C.-C. Wu, 2008: A numerical study of the track deflection of Supertyphoon Haitang (2005) prior to its landfall in Taiwan. *Mon. Wea. Rev.,* **136,** 598–615, doi:10.1175/2007MWR2134.1.

Jordan, C. L., 1958: Mean soundings for the West Indies area. *J. Meteor.,* **15,** 91–97, doi:10.1175/1520-0469(1958)015<0091:MSFTWI>2.0.CO;2.

Kossin, J. P., J. A. Knaff, H. I. Berger, D. C. Herndon, T. A. Cram, C. S. Velden, R. J. Murnane, and J. D. Hawkins, 2007: Estimating hurricane wind structure in the absence of aircraft reconnaissance. *Wea. Forecasting,* **22,** 89–101, doi:10.1175/WAF985.1.

Kuo, H.-C., R. T. Williams, J.-H. Chen, and Y.-L. Chen, 2001: Topographic effects on barotropic vortex motion: No mean flow. *J. Atmos. Sci.,* **58,** 1310–1327, doi:10.1175/1520-0469(2001)058<1310:TEOBVM>2.0.CO;2.

Lin, Y.-L., 2007: *Mesoscale Dynamics.* Cambridge University Press, 630 pp.

——, and L. C. Savage III, 2011: Effects of landfall location and the approach angle of a cyclone vortex encountering a mesoscale mountain range. *J. Atmos. Sci.,* **68,** 2095–2106, doi:10.1175/2011JAS3720.1.

——, J. Han, D. W. Hamilton, and C.-Y. Huang, 1999: Orographic influence on a drifting cyclone. *J. Atmos. Sci.,* **56,** 534–562, doi:10.1175/1520-0469(1999)056<0534:OIOADC>2.0.CO;2.

——, S.-Y. Chen, C. M. Hill, and C.-Y. Huang, 2005: Control parameters for the influence of a mesoscale mountain range on cyclone track continuity and deflection. *J. Atmos. Sci.,* **62,** 1849–1866, doi:10.1175/JAS3439.1.

Roux, F., and F. D. Marks Jr., 1991: Eyewall evolution in Hurricane Hugo deduced from successive airborne Doppler observations. Preprints, *19th Conf. on Hurricanes and Tropical Meteorology,* Miami, FL, Amer. Meteor. Soc., 558–563.

Smith, R. B., and D. F. Smith, 1995: Pseudoinviscid wake formation by mountains in shallow-water flow with a drifting vortex. *J. Atmos. Sci.,* **52,** 436–454, doi:10.1175/1520-0469(1995)052<0436:PWFBMI>2.0.CO;2.

Smolarkiewicz, P. K., and R. Rotunno, 1989: Low Froude number flow past three-dimensional obstacles. Part I: Baroclinically generated lee vortices. *J. Atmos. Sci.,* **46,** 1154–1164, doi:10.1175/1520-0469(1989)046<1154:LFNFPT>2.0.CO;2.

Tang, C. K., and J. C. L. Chan, 2013: Idealized simulations of the effect of Taiwan and Philippines topographies on tropical cyclone tracks. *Quart. J. Roy. Meteor. Soc.,* **140,** 1578–1589, doi:10.1002/qj.2240.

Wang, S.-T., 1980: Prediction of the movement and strength of typhoons in Taiwan and its vicinity (in Chinese). National Science Council Research Rep. 108, 100 pp.

Willoughby, H. E., and M. E. Rahn, 2004: Parametric representation of the primary hurricane vortex. Part I: Observations and evaluation of the Holland (1980) model. *Mon. Wea. Rev.,* **132,** 3033–3048, doi:10.1175/MWR2831.1.

Wu, C.-C., 2001: Numerical simulation of Typhoon Gladys (1994) and its interaction with Taiwan terrain using the GFDL hurricane model. *Mon. Wea. Rev.,* **129,** 1533–1549, doi:10.1175/1520-0493(2001)129<1533:NSOTGA>2.0.CO;2.

——, 2013: Typhoon Morakot: Key findings from the journal *TAO* for improving prediction of extreme rains at landfall. *Bull. Amer. Meteor. Soc.,* **94,** 155–160, doi:10.1175/BAMS-D-11-00155.1.

——, and K. A. Emanuel, 1995a: Potential vorticity diagnostics of hurricane movement. Part I: A case study of Hurricane Bob (1991). *Mon. Wea. Rev.,* **123,** 69–92, doi:10.1175/1520-0493(1995)123<0069:PVDOHM>2.0.CO;2.

——, and ——, 1995b: Potential vorticity diagnostics of hurricane movement. Part II: Tropical Storm Ana (1991) and Hurricane Andrew (1992). *Mon. Wea. Rev.,* **123,** 93–109, doi:10.1175/1520-0493(1995)123<0093:PVDOHM>2.0.CO;2.

——, and Y.-H. Kuo, 1999: Typhoons affecting Taiwan: Current understanding and future challenges. *Bull. Amer. Meteor. Soc.,* **80,** 67–80, doi:10.1175/1520-0477(1999)080<0067:TATCUA>2.0.CO;2.

Yeh, T.-C., and R. L. Elsberry, 1993: Interaction of typhoons with the Taiwan orography. Part I: Upstream track deflections. *Mon. Wea. Rev.,* **121,** 3193–3212, doi:10.1175/1520-0493(1993)121<3193:IOTWTT>2.0.CO;2.

Zhang, D., and R. A. Anthes, 1982: A high-resolution model of the planetary boundary layer—Sensitivity tests and comparisons with SESAME-79 data. *J. Appl. Meteor.,* **21,** 1594–1609, doi:10.1175/1520-0450(1982)021<1594:AHRMOT>2.0.CO;2.